IEEE Access
Multidisciplinary | Rapid Review | Open Access Journal

Received July 21, 2017, accepted August 13, 2017, date of publication August 21, 2017, date of current version September 19, 2017.

Digital Object Identifier 10.1109/ACCESS.2017.2740498

On the Multiband Carrier Aggregated Nonlinear LTE-A System

PARAG AGGARWAL AND VIVEK ASHOK BOHARA

Wirocomm Research Group, Department of Electronics and Communication, Indraprastha Institute of Information Technology-Delhi (IIIT-Delhi), New Delhi 110020, India

Corresponding author: Parag Aggarwal (paraga@iiitd.ac.in)

ABSTRACT This paper analyzes the impact of nonlinear high power amplifiers (HPAs) on the multiband carrier aggregated (CA) long-term evolution-advanced (LTE-A) system. It is assumed that the LTE-A system consists of a multi-input-multioutput (MIMO) orthogonal frequency-division multiplexing (OFDM)-based downlink physical-layer architecture. It has been shown that the nonlinear distortion caused by HPAs can be represented in terms of a complex attenuation factor and additive zero mean Gaussian ''nonlinear" noise. The closed-form generalized expressions of complex attenuation factor and variance of additive Gaussian nonlinear noise are derived that are applicable to any number of aggregated bands with any nonlinearity order and memory depth. From these expressions, the overall performance of a multiband CA-MIMO-OFDM system in terms of symbol error rate and error vector magnitude for M-ary quadrature amplitude modulation (M-QAM) has been evaluated. We also investigate the combined effect of a number of aggregated bands, input-back off, and diversity gain on the performance of a CA-MIMO-OFDM system. It is observed that diversity gain can improve the performance of CA-MIMO-OFDM in low signal-to-noise ratio (SNR) region. However, in the high SNR region, there is no substantial effect of increasing diversity on the performance. A good agreement between the analytical and simulation results in the multipath Rayleigh fading channel validates the theoretical results obtained in this paper.

INDEX TERMS LTE-A, carrier aggregation, OFDM, MIMO, high power amplifier, nonlinear distortion, EVM.

I. INTRODUCTION

Long Term Evolution-Advanced (LTE-A) is an enhancement of LTE and has been standardised by 3rd Generation Partnership Project (3GPP) in LTE Release-10 [1]. It provides high peak data rates, flexible spectrum operations, improved system capacity, large coverage and is compatible with existing systems. It inherits all features of LTE, however its own unique features such as carrier aggregation, device-to-device communication, advanced antenna techniques, heterogeneous networks (HetNets), etc., attract the attention of most researchers.

Carrier Aggregation (CA) which has been incorporated as one of the feature of LTE-A standard was proposed to enhance the data rates of existing LTE systems. It allows scalable widening of effective bandwidth by combining the multiple carriers to support wideband signals [2], [3]. These carriers may be in the same or different bands, and may be of different bandwidths to provide maximum flexibility in utilizing the scarce radio spectrum. There are three types of CA depending on the continuity and positioning of the bands: Intra-band contiguous (carriers are continuous and present in same frequency band), Intra-band non-contiguous (carriers are non-continuous but present in same frequency band), and Inter-band non-contiguous (carriers are present in different frequency bands). In 4G LTE-A, up to five carriers each having a maximum bandwidth of 20MHz can be aggregated together to get wide bandwidth of maximum 100MHz, while in LTE-A Pro (4.5G, comprising LTE Releases 13 and 14), beyond five carriers for CA are considered and up to 32 carriers can be aggregated which is known as massive or enhanced CA (MCA or eCA) [4]. Moreover, MCA allows CA within licensed spectrum and/or unlicensed spectrum, which supports downlink peak data rate up to 25 Gb/s.

Orthogonal frequency division multiplexing (OFDM) is a multi-carrier modulation technique which provides high spectral efficiency along with immunity to frequency selective fading channels, and tolerance to multi-path delay spread [5]. Consequently, OFDM and its variants have been widely used in various wireless standards to provide high data rate communication. Moreover, MIMO systems provide

high throughput and transmission reliability in fading channel by virtue of diversity and multiplexing gains. Since OFDM and MIMO are complimentary techniques, a MIMO-OFDM system is widely used in many wireless applications including LTE-A standard [6]. However, OFDM consists of large number of independent subcarriers which means that the resultant signal has significant peak-to-average power ratio (PAPR). Incorporation of additional features like MIMO and CA further increases the PAPR of OFDM signal [7], [8].

CA-MIMO-OFDM system comprises of three prominent features of 4G LTE-A: MIMO is used to provide diversity and multiplexing gain, CA yields wide bandwidth, and OFDM mitigates the multi-path fading. However like the conventional MIMO-OFDM system, CA-MIMO-OFDM system is also vulnerable to nonlinear distortion caused by HPAs. HPAs are conventionally designed to operate near saturation region in order to attain maximum efficiency. When a CA-MIMO-OFDM signal with high PAPR is passed through a HPA, it leads to significant in-band and out-of-band distortions at the output. These distortions cause spectral regrowth, low efficiency, performance degradation, interference to other systems, and system capacity loss. To mitigate this distortion, HPAs can be operated with high backoff, however it compromises their power efficiency.

Sufficient amount of research has been devoted to study the effects of nonlinear distortion caused by HPA when driven with high PAPR signal [9]–[13]. In [9], the analysis of PA nonlinearity was based on the application of Bussgang's Theorem with complex Gaussian non zero-mean input signals. Authors in [10], [11] and [12], [13] used the statistical approach to model the nonlinear distortion caused by HPA without memory effects and with memory effects, respectively. The above analysis was extended for MIMO-OFDM systems in [14]–[16]. For instance, the impact of nonlinear HPA on MIMO-OFDM system with zero forcing equalization was investigated in [14]. The error performance of MIMO systems with transmit beamforming and single value decomposition (SVD) were analysed in [15] and [16], respectively. These analysis also showed the effect of number of transmit antennas on the nonlinear distortion caused by HPA.

CA allows multiple frequency bands to be aggregated together to transmit wideband signals. However, unlike the conventional single-band OFDM system, when CA-OFDM signals are passed through a nonlinear HPA, it produces cross-modulation terms apart from conventional intermodulation and out-of-band distortion terms. These cross-modulation terms further degrades the performance of CA-OFDM system. As a consequence, the conventional analysis on a single band nonlinear OFDM system [14]–[16] may not be applicable to CA-OFDM signal. In [17]–[19], the performance of CA-OFDM system was evaluated in the presence of nonlinear HPA. However, due to the complexity of the derived expressions, their analysis was restricted to 3^{rd} order nonlinearity and single-input-single-output (SISO) systems. In [20], [21], authors extended the analysis of [18] by adding more levels of nonlinearity for dual band CA signals. However, generalized expressions for multi-band CA-OFDM systems where more than two bands are aggregated together were not derived.

Further most of the previous analysis were limited to deriving the numerical expressions of symbol error rate, however performance evaluation in terms of EVM was often overlooked. Since, nonlinearity causes rotation and compression/expansion of the signal constellation, so EVM can be used as an alternative performance metric as it has an information about the signals phase and amplitude errors [22]–[25]. EVM is basically a measure of errors between the received symbols and expected symbols. It quantifies the error in the departure of signals constellation from its ideal reference because of nonlinearity. Along with SER, it is an important performance metric of wireless communication system. Further, EVM requires less complex processing than SER because to calculate SER, the received signal has to follow the whole receiver process but in case of EVM, it can be calculated before demodulation. In [19], authors analysed the SISO dual band CA OFDM system in terms of EVM in the presence of multi-path Rayleigh fading channel. However, the analysis in [19] is also limited to dual band CA systems and moreover, MIMO system was not considered.

A. CONTRIBUTION

In this paper we have analyzed the impact of nonlinear HPA on multi-band CA-MIMO-OFDM system, a topic which has been overlooked so far. The nonlinear behavior of the HPA has been modeled by a multi-band generalized memory polynomial (MB-GMP) model. It has been shown that the received symbol after downconversion can be canonically decomposed into complex attenuation factor and additive nonlinear noise. Unlike [20], [21], the generalised mathematical expressions of complex attenuation factor and additive nonlinear noise for any number of aggregated bands with any nonlinearity order and any memory depth of HPA have been derived.

The proposed work also provides valuable insights on the impact of number of aggregated carriers on the error performance of a nonlinear CA-MIMO-OFDM system.[1] It has been shown that the nonlinear noise is a function of number of aggregated carriers and increases as the number of aggregated carriers increases. Further, this nonlinear noise also impact the diversity order of a nonlinear CA-MIMO-OFDM system. Although the performance of a CA-MIMO-OFDM improves by increasing diversity gain in low SNR regime, it has been shown that there is no substantial impact of increasing diversity on higher SNR regime.

In addition to above, generalised expression of EVM of a nonlinear CA-MIMO-OFDM system in the multi-path Rayleigh fading channel has been derived. This expression is valid for any number of aggregated bands, any number of transmit/receive antennas, any nonlinearity order or memory

[1]For brevity, we denote a CA-MIMO-OFDM system in the presence of nonlinear HPA as a nonlinear CA-MIMO-OFDM system.

depth. Finally, simulation results are presented to validate the efficacy of the proposed analysis by comparing it with the analytically obtained expressions.

Some of the significant contributions of the proposed work are summarized as below:

- Generalised expressions of complex attenuation factor and additive nonlinear noise for any number of aggregated bands with any nonlinearity order and any memory depth of HPA have been derived.
- From the derived expressions, an analytical methodology has been proposed to obtain the received SNR and SER of a nonlinear CA-MIMO-OFDM system.
- The closed form expression for EVM at both transmitter and receiver has also been derived for nonlinear CA-MIMO-OFDM system
- Impact of number of aggregated carriers on SER and EVM of CA-MIMO-OFDM system is investigated. It has been shown that the SER and EVM degrades with the number of aggregated carriers.
- Effect of diversity order on the performance of CA-MIMO-OFDM system has been investigated. Although the performance of CA-MIMO-OFDM can be improved by increasing diversity gain in low SNR regime, there is no substantial impact of increasing diversity on higher SNR regime.

The rest of the paper is organised as follows: Section II presents the system model. Section III describes the theoretical approach of CA-MIMO-OFDM system. The derivation of SER and EVM are provided in Section IV and V, respectively. The numerical and simulation results are presented in Section VI. Finally, Section VII concludes the paper.

Notations: Vectors and matrices are denoted by lower and upper case bold-face letters, respectively. E[·] denotes the expectation operator, and (·)! refers to the factorial operator. $(\cdot)^*$, $(\cdot)^T$, $(\cdot)^H$, and $(\cdot)^{-1}$ represent the conjugate, transpose, Hermitian, and inverse operators, respectively. $\mathcal{CN}(m, \sigma^2)$ represents the complex Gaussian distribution with m mean and σ^2 variance.

II. SYSTEM MODEL

This section presents the CA-OFDM system model, behavioral model for multi-band HPAs, and multi-path Rayleigh fading MIMO channel model.

A. MIMO CHANNEL

The MIMO system consists of N_T transmit antennas and N_R receive antennas. The channel is assumed to be a wide sense stationary uncorrelated scattering (WSSUS) Rayleigh fading channel [13]. The equivalent channel model can be represented as

$$\mathbf{H}[n] = \sum_{l=1}^{L} \hat{\mathbf{H}}_l \delta[n-l], \tag{1}$$

where $\mathbf{H}[n]$ is the MIMO channel response, L is total number of delay taps, and $\hat{\mathbf{H}}_l$ contains the MIMO channel coefficients

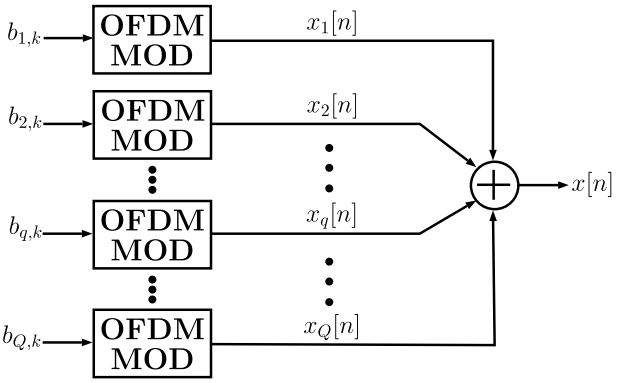

FIGURE 1. CA-OFDM signal with aggregation of Q bands.

for the l^{th} multi-path which can be written as

$$\hat{\mathbf{H}}_l = \begin{bmatrix} h_{1,1,l} & h_{1,2,l} & \cdot\cdot & h_{1,N_T,l} \\ h_{2,1,l} & h_{2,2,l} & \cdot\cdot & h_{2,N_T,l} \\ \cdot & \cdot & \cdot\cdot & \cdot \\ \cdot & \cdot & \cdot\cdot & \cdot \\ h_{N_R,1,l} & h_{N_R,2,l} & \cdot\cdot & h_{N_R,N_T,l} \end{bmatrix}_{N_R \times N_T} \tag{2}$$

where $h_{i,j,l}$ is the channel impulse response between j^{th} transmitting antenna and i^{th} receive antenna for l^{th} delay tap. We assume that the channel is perfectly known at the receiver to decode the transmit signals.

B. CA-OFDM SIGNAL

A CA-OFDM signal $x[n]$ consists of multiple component carriers (CCs) that are aggregated together to transmit wideband signals. Each CC has an OFDM modulator which modulates the incoming complex data symbols into OFDM symbols $x_q[n]$ at q^{th} carrier. The CCs are aggregated together using power combiner as shown in Fig. 1. Each OFDM modulator consists of serial-to-parallel convertor, inverse discrete fourier transform (IDFT), cyclic prefix adder and parallel-to-serial converter blocks. The baseband equivalent expression of OFDM symbol with N subcarriers, appended with the guard interval, N_g, and the discrete time index n can be represented as [10]:

$$x_q^j[n] = \frac{1}{N} \sum_{k=0}^{N-1} b_{q,k}^j e^{j2\pi kn/N}, \quad -N_g \le n \le N-1 \tag{3}$$

where $x_q^j[n]$ is the OFDM symbol input to the HPA of j^{th} transmitting antenna at q^{th} component carrier, $b_{q,k}^j$ is the complex data symbol on k^{th} subcarrier of the OFDM symbol at q^{th} component carrier. Without loss of generality, it is presumed that complex data symbols $b_{q,k}^j$ are independent and identically distributed with zero mean and variance P_b. By the Central Limit Theorem (CLT) [26], when the number of subcarriers N is large, $x_q^j[n]$ can be assumed to be a complex Gaussian process with zero mean and variance $P_{av} = P_b/N$.

C. BEHAVIORAL MODEL FOR HPA

Several behavioral models such as Wiener, Hammerstein, Wiener-Hammerstein, parallel Wiener, memory polyno-

mial (MP), GMP have been conventionally used in literature to characterise the nonlinear behavior of HPAs [27]–[29]. Through judicious selection of parameters, these models were able to capture the in-band and out-of-band distortions caused due to nonlinear HPA on a single-band OFDM transmitters. However, when a CA signal is passed through nonlinear HPA, the signals from one component carrier may interfere with other which introduce the cross-modulation products in addition to in-band and out-of-band intermodulation products. As a consequence, conventional HPA models are not adequate to capture the nonlinear behavior of HPA in CA system. To account for these intermodulation and cross modulation effects, more generalised model is required.

With respect to above, in [17] and [18], [21] two-dimensional (2D) enhanced Hammerstein (EH) and 2D-MP model have been used respectively to characterize the nonlinear distortion caused by HPAs on aggregation of dual carriers. However, 2D-GMP is restricted in a sense as it can be only used to model the nonlinear distortion of HPA when excited by dual band CA-OFDM signal [20]. It can be extended for Q number of bands by including more cross modulation products. The resultant model is termed as MB-GMP and can be expressed as (4), as shown at the bottom of this page where, $y_q^j[n]$ is the output of the nonlinear HPA of the j^{th} transmitting antenna corresponding to the input signal $x_q^j[n]$ in q^{th} frequency band. P denotes the nonlinearity order, M is the memory depth and G is the number of cross terms. $a^j_{p_1,p_2,\cdots,p_Q,m,g}$ are the complex nonlinearity coefficients of HPA for p_q^{th} order nonlinearity and m^{th} memory depth with g^{th} cross term [29]. The frequency separations between the aggregated bands are assumed to be large so that the out-of-band distortion lie far from operating frequencies and can easily be filtered out [30]. Hence the current analysis is restricted to in-band distortions.

III. CA-MIMO-OFDM SYSTEM

The schematic of CA-MIMO-OFDM system is shown in Fig. 2. Each CA-OFDM signal is passed through a nonlinear HPA at each transmitter.

At receiver, multiple antennas receive signals from each Tx antenna. The baseband representation of a received signal vector for q^{th} band can be expressed as[2]

$$\mathbf{r}_q[n] = \sum_{l=1}^{L} \hat{\mathbf{H}}_l \mathbf{y}_q[n-l] + \mathbf{w}[n], \tag{5}$$

[2]Although the analytical results have been obtained for q^{th} component carrier, however the aforementioned analysis is applicable to any component carrier.

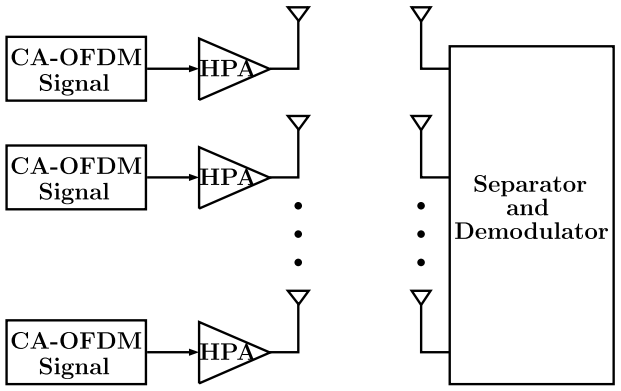

FIGURE 2. Schematic of CA-MIMO-OFDM system.

where $\mathbf{r}_q[n]$ is a $N_R \times 1$ vector of received signals that are present in q^{th} frequency band, $\mathbf{y}_q[n]$ is a $N_T \times 1$ transmit signal vector at the output of HPA for q^{th} frequency band, $\mathbf{w}[n]$ is a $N_R \times 1$ noise vector whose components $n_o^i \sim \mathcal{CN}(0, N_o)$ are the additive white Gaussian noise (AWGN), and N_o is AWGN variance. The signal in i^{th} receive antenna is given as

$$r_q^i[n] = \sum_{j=0}^{N_T-1} \sum_{l=0}^{L-1} h_{i,j,l} y_q^j[n-l] + w^i[n]. \tag{6}$$

On substituting (4) into (6), we get

$$\begin{aligned} & r_q^i[n] \\ &= \sum_{j=0}^{N_T-1} \sum_{l=0}^{L-1} h_{i,j,l} \sum_{p_1=1}^{P} \sum_{p_2=1}^{p_1} \cdots \sum_{p_Q=1}^{p_{Q-1}} \sum_{m=0}^{M-1} \sum_{g=-G}^{G} \\ & a^j_{p_1,p_2,\cdots,p_Q,m,g}\, x_q^j[n-m-l] \left|x_1^j[n-m-g-l]\right|^{p_1-p_2} \\ & \cdots \left|x_Q^j[n-m-g-l]\right|^{p_Q-1} + w^i[n]. \end{aligned} \tag{7}$$

After removal of cyclic prefix and applying DFT, the received complex data symbols at k^{th} subcarrier can be expressed as

$$\begin{aligned} & r^i_{q,k} \\ &= \sum_{j=0}^{N_T-1} \sum_{l=0}^{L-1} h_{i,j,l} \sum_{n=0}^{N-1} \sum_{p_1=1}^{P} \sum_{p_2=1}^{p_1} \cdots \sum_{p_Q=1}^{p_{Q-1}} \sum_{m=0}^{M-1} \sum_{g=-G}^{G} \\ & a^j_{p_1,p_2,\cdots,p_Q,m,g}\, x_q^j[n-m-l] \left|x_1^j[n-m-g-l]\right|^{p_1-p_2} \\ & \cdots \left|x_Q^j[n-m-g-l]\right|^{p_Q-1} e^{-j2\pi kn/N} + w^i_k, \end{aligned} \tag{8}$$

where w^i_k is the noise term at k^{th} subcarrier in i^{th} receive branch. Using circular time shift property of DFT, (8) can be

$$y_q^j[n] = \sum_{p_1=1}^{P} \sum_{p_2=1}^{p_1} \cdots \sum_{p_Q=1}^{p_{Q-1}} \sum_{m=0}^{M-1} \sum_{g=-G}^{G} a^j_{p_1,p_2,\cdots,p_Q,m,g} x_q^j[n-m] \left|x_1^j[n-m-g]\right|^{p_1-p_2} \cdots \left|x_Q^j[n-m-g]\right|^{p_Q-1} \tag{4}$$

$$\mu_{q,k}^{j} = \sum_{p_1=1}^{P}\sum_{p_2=1}^{p_1}\cdots\sum_{p_Q=1}^{p_{Q-1}}\left(\frac{P_b}{N}\right)^{\frac{p_1-1}{2}}\left(\alpha_{p_1,p_2,\cdots,p_Q,k,0}^{j}\Gamma\left(1+\frac{p_1-p_2}{2}\right)\cdots\Gamma\left(1+\frac{p_q-p_{q+1}+2}{2}\right)\right.$$
$$\left.\cdots\Gamma\left(1+\frac{p_Q-1}{2}\right)+\sum_{\substack{g=-G\\ g\neq 0}}^{G}\alpha_{p_1,p_2,\cdots,p_Q,k,g}^{j}\Gamma(2)\,\Gamma\left(1+\frac{p_1-p_2}{2}\right)\cdots\Gamma\left(1+\frac{p_Q-1}{2}\right)\right), \quad (15)$$

$$\eta_{q,k}^{j} = \sum_{n=0}^{N-1}\sum_{p_1=1}^{P}\sum_{p_2=1}^{p_1}\cdots\sum_{p_Q=1}^{p_{Q-1}}\sum_{g=-G}^{G}\alpha_{p_1,p_2,\cdots,p_Q,k,g}^{j}x_q^j[n+g]\left|x_1^j[n]\right|^{p_1-p_2}\cdots\left|x_Q^j[n]\right|^{p_Q-1}e^{-j2\pi k(n+g)/N}-\mu_{q,k}^{j}b_{q,k}^{j}. \quad (16)$$

rewritten as

$$r_{q,k}^{i} = \sum_{j=0}^{N_T-1}\sum_{l=0}^{L-1}h_{i,j,l}\sum_{n=0}^{N-1}\sum_{p_1=1}^{P}\sum_{p_2=1}^{p_1}\cdots\sum_{p_Q=1}^{p_{Q-1}}\sum_{m=0}^{M-1}\sum_{g=-G}^{G}$$
$$a_{p_1,p_2,\cdots,p_Q,m,g}^{j}\,x_q^j[n+g]\left|x_1^j[n]\right|^{p_1-p_2}\cdots\left|x_Q^j[n]\right|^{p_Q-1}$$
$$e^{-j2\pi k(n+m+g+l)/N}+w_k^i. \quad (9)$$

After rearranging (9), we obtain

$$r_{q,k}^{i} = \sum_{j=0}^{N_T-1}\overline{h}_{i,j,k}s_{q,k}^{j}+w_k^i, \quad (10)$$

where $\overline{h}_{i,j,k}$ is the effective channel coefficient from j^{th} transmit antenna to i^{th} receive antenna of k^{th} subcarrier and can be written as

$$\overline{h}_{i,j,k} = \sum_{l=0}^{L-1}h_{i,j,l}e^{-j2\pi kl/N}, \quad (11)$$

and $s_{q,k}^{j}$ is the complex data symbol affected by nonlinear distortion only, i.e.,

$$s_{q,k}^{j} = \sum_{n=0}^{N-1}\sum_{p_1=1}^{P}\sum_{p_2=1}^{p_1}\cdots\sum_{p_Q=1}^{p_{Q-1}}\sum_{g=-G}^{G}\alpha_{p_1,p_2,\cdots,p_Q,k}^{j}$$
$$x_q^j[n+g]\left|x_1^j[n]\right|^{p_1-p_2}\cdots\left|x_Q^j[n]\right|^{p_Q-1}e^{-j2\pi k(n+g)/N}, \quad (12)$$

where

$$\alpha_{p_1,p_2,\cdots,p_Q,k,g}^{j} = \sum_{m=0}^{M-1}a_{p_1,p_2,\cdots,p_Q,m,g}^{j}e^{-j2\pi km/N}. \quad (13)$$

Proposition 1: The received complex data symbol $s_{q,k}^{j}$ in (12) can be canonically decomposed as complex attenuation factor $\mu_{q,k}^{j}$ multiplied to the desired data symbol $b_{q,k}^{j}$ and additive nonlinear noise $\eta_{q,k}^{j}$, and is given as

$$s_{q,k}^{j} = \mu_{q,k}^{j}b_{q,k}^{j}+\eta_{q,k}^{j}, \quad (14)$$

Proof: The proof is given in Appendix A. ■

The generalised expressions of complex attenuation factor $\mu_{q,k}^{j}$ and nonlinear noise $\eta_{q,k}^{j}$ can be expressed in (15) and (16), as shown at the top of the page, respectively.

It is noticeable that the value of $\mu_{q,k}^{j}$ depends on both linear and nonlinear coefficients and it acts as gain of HPA, while $\eta_{q,k}^{j}$ strictly depends on the nonlinear coefficients and acts as interference to an information signal. As mentioned earlier that the number of nonlinear coefficients (cross-modulation terms) increase with number of aggregated bands. As a consequence, the value of $\eta_{q,k}^{j}$ increases with number of aggregated bands which affects the performance of CA-MIMO-OFDM system.

Proposition 2: The nonlinear noise term $\eta_{q,k}^{j}$ can be approximated as a complex Gaussian process $\mathcal{CN}(0,\sigma^2_{\eta_{q,k}^{j}})$ for a sufficiently large value of N.

Proof: The proofs are given in Appendix B and C. ■

Using (10) and (14), the received complex data symbol at k^{th} subcarrier of i^{th} receive antenna can be written as

$$r_{q,k}^{i} = \sum_{j=0}^{N_T-1}\overline{h}_{i,j,k}\left(\mu_{q,k}^{j}b_{q,k}^{j}+\eta_{q,k}^{j}\right)+w_k^i. \quad (17)$$

From (17), it is quite obvious that the equivalent system of the k^{th} subcarrier in q^{th} frequency band is a MIMO system which can be expressed as

$$\mathbf{r}_{q,k} = \mathbf{H}_k\mathbf{s}_{q,k}+\mathbf{w}_k, \quad (18)$$

where $\mathbf{r}_{q,k} = [r_{q,k}^1, r_{q,k}^2, \ldots, r_{q,k}^{N_R}]^T$, $\mathbf{s}_{q,k} = [s_{q,k}^1, s_{q,k}^2, \ldots, s_{q,k}^{N_T}]^T$, $\mathbf{w}_k = [w_k^1, w_k^2, \ldots, w_k^{N_R}]^T$ and H_k is $N_R \times N_T$ effective channel whose components are $\overline{h}_{i,j,k}$. We assume that the transmit vector of complex data symbols can be estimated at the receiver using zero forcing equalization [31] through

$$\hat{\mathbf{b}}_{q,k} = \mathbf{s}_{q,k}+\mathbf{H}_k^{\dagger}\mathbf{w}_k, \quad (19)$$

where $\hat{\mathbf{b}}_{q,k} = [\hat{b}_{q,k}^1, \hat{b}_{q,k}^2, \ldots, \hat{b}_{q,k}^{N_T}]^T$ is a vector of estimated transmitted data symbols and $\mathbf{H}_k^{\dagger}$ is a pseudo inverse of the channel matrix $\mathbf{H}_k$ at the k^{th} subcarrier.

IV. SER ANALYSIS

In this section, we measure the performance of CA-MIMO-OFDM system in terms of symbol error rate (SER) in the

presence of multi-path Rayleigh fading channel. Using (14) and (19), the j^{th} estimated data symbol at the k^{th} subcarrier in q^{th} frequency band can be written as

$$\hat{b}^j_{q,k} = \mu^j_{q,k} b^j_{q,k} + \eta^j_{q,k} + \left[\mathbf{H}^{\dagger}_k w_k\right]^j, \tag{20}$$

where $\left[\mathbf{H}^{\dagger}_k w_k\right]^j$ is j^{th} element of vector $\mathbf{H}^{\dagger}_k w_k$. The resultant signal-to-noise ratio (SNR) for each subcarrier can be expressed as

$$\begin{aligned}\Upsilon^j_{q,k} &= \frac{P_b \left|\mu^j_{q,k}\right|^2}{\sigma^2_{\eta^j_{q,k}} + \left[\left((\mathbf{H}_k)^H \mathbf{H}_k\right)^{-1}\right]^j N_o}, \\ &= \frac{\Upsilon_o}{\gamma^j_{q,k} + \frac{1}{\phi_k}} \left|\mu^j_{q,k}\right|^2, \end{aligned} \tag{21}$$

where

$$\Upsilon_o = \frac{P_b}{N_o}, \quad \gamma^j_{q,k} = \frac{\sigma^2_{\eta^j_{q,k}}}{N_o}, \tag{22}$$

and

$$\phi_k = \frac{1}{\left[\left((\mathbf{H}_k)^H \mathbf{H}_k\right)^{-1}\right]^j}. \tag{23}$$

ϕ_k has a Chi-squared distribution with $2(N_R - N_T + 1)$ degrees of freedom and can be expressed as [31]

$$p_{\phi_k}(\phi_k) = \frac{\phi_k^{(N_R - N_T)}}{\Phi_k^{(N_R - N_T + 1)} (N_R - N_T)!} e^{-\frac{\phi_k}{\Phi_k}}, \tag{24}$$

where, $\Phi_k = \underset{\phi_k}{E}[\phi_k]$. Using (21), SER of the received symbol for M-QAM can be expressed as [32]

$$f^j_{q,k}(\phi_k) = 1 - \left(1 - \left(1 - \frac{1}{\sqrt{M}}\right) erfc\left(\sqrt{\frac{3\Upsilon^j_{q,k}}{2\,(M-1)}}\right)\right)^2 \tag{25}$$

where, *erfc* is an error function [32]. Therefore, the SER averaged across the fading channel can be expressed as:

$$SER^j_{q,k} = \mathrm{E}\left[f^j_{q,k}(\phi_k)\right] = \int_0^\infty f^j_{q,k}(\phi_k) p_{\phi_k}(\phi_k) d\phi_k. \tag{26}$$

The average SER across all the subcarriers and all transmitting branches thus can be calculated as:

$$SER_q = \frac{1}{N_T N} \sum_{j=0}^{N_T - 1} \sum_{k=0}^{N-1} SER^j_{q,k}. \tag{27}$$

The analytical expression (26) is intractable and hence is evaluated using numerical methods. (26)-(27) provides the complete analysis of CA-MIMO-OFDM system in the presence of nonlinear HPA in terms of SER over the multi-path Rayleigh fading channel.

It is well known fact that SER improves with increase in transmit power and diversity gain for the case of ideal linear HPA. However, due to the impact of nonlinear HPA, it can be observed from (21) that received SNR is affected by two type of noises: 1) AWGN and 2) Nonlinear noise. In low SNR regime, AWGN dominates the nonlinear noise ($\sigma^2_\eta << N_o$) and the system performance improves with increase in SNR and diversity gain. In high SNR regime, nonlinear noise dominates the AWGN ($\sigma^2_\eta >> N_o$) which leads to irreducible error floor.

V. EVM ANALYSIS

In this section, the performance of CA-MIMO-OFDM system has been analysed in terms of EVM. EVM can be defined in terms of received SNR as [24]

$$EVM = \frac{1}{\sqrt{\Upsilon^j_{q,k}}}. \tag{28}$$

Using (21) and (28), EVM for each subcarrier in q^{th} frequency band of CA-MIMO-OFDM system with nonlinear HPA in the presence of multi-path Rayleigh fading channel can be written as:

$$EVM^j_{q,k}(\phi_k) = \frac{1}{\sqrt{\Upsilon_o \left|\mu^j_{q,k}\right|^2}} \sqrt{\gamma^j_{q,k} + \frac{1}{\phi_k}}. \tag{29}$$

For each subcarrier, EVM is obtained by averaging across Rayleigh fading channel and can be expressed as

$$EVM^j_{q,k} = \int_0^\infty EVM^j_{q,k}(\phi_k) p_{\phi_k}(\phi_k) d\phi_k. \tag{30}$$

Using (29) and (30), we have

$$EVM^j_{q,k} = \sqrt{\frac{\gamma^j_{q,k}}{\Upsilon_o \left|\mu^j_{q,k}\right|^2} I^j_{q,k}}, \tag{31}$$

where

$$I^j_{q,k} = \int_0^\infty \sqrt{\frac{1 + \phi_k \gamma^j_{q,k}}{\phi_k \gamma^j_{q,k}}} p_{\phi_k}(\phi_k) d\phi_k. \tag{32}$$

On using (22) and substituting $\phi_k \gamma^j_{q,k} = \beta$, (32) can be rewritten as

$$\begin{aligned} I^j_{q,k} &= \frac{1}{(N_R - N_T)! \left(\gamma^j_{q,k} \Phi_k\right)^{N_R - N_T + 1}} \\ &\quad \times \int_0^\infty (\beta + 1)^{\frac{1}{2}} \beta^{N_R - N_T - \frac{1}{2}} e^{-\frac{\beta}{\gamma^j_{q,k} \Phi}} d\beta \\ &= \frac{1}{\Gamma\left(N_R - N_T + \frac{1}{2}\right)(N_R - N_T)! \left(\gamma^j_{q,k} \Phi_k\right)^{N_R - N_T + 1}} \\ &\quad \times U\left(N_R - N_T + \frac{1}{2}, N_R - N_T + 2, \frac{1}{\gamma^j_{q,k} \Phi_k}\right), \end{aligned} \tag{33}$$

where U is the Confluent Kummer hypergeometric function [33] which is given as,

$$U(a, b, c) = \frac{1}{\Gamma(a)} \int_0^\infty e^{-ct} t^{a-1} (1 + t)^{b-a-1} dt, \tag{34}$$

where $\Gamma(a)$ is the gamma function. Using (22), (31) and (33), the closed form expression of average EVM in q^{th} frequency band across all the subcarriers and all transmitting branch can be given as (35), as shown at the bottom of the page.

VI. SIMULATION RESULTS

In this section, simulation results are presented to evaluate the performance of CA-MIMO-OFDM system impaired by nonlinear HPA with memory. As discussed before, the propagation channel has been modeled as a multi-path Rayleigh fading channel. The simulations have also been compared with theoretical results to validate the analytically obtained expressions. Specifically, the performance has been evaluated by calculating the signal-to-distortion-noise ratio (SDNR), SER and EVM of the received CA-OFDM signal. Further, the impact of number of aggregated bands on the diversity order on CA-MIMO-OFDM system has also been investigated.

The nonlinear HPA is modeled by MB-GMP model with 3^{rd} order nonlinearity ($P = 3$), $M = 4$ and $G = 2$. For ease of simulations, it is assumed that HPAs in all transmitters have same behavioral characteristics [16]. The performance of a communication system in the presence of nonlinear HPA is usually quantified by input-back-off (IBO), i.e., IBO $= \frac{A^2}{P_{av}}$ where, A is the input saturation voltage of HPA [10]. Thus, higher the IBO, less is the impact of nonlinear distortions as HPA tends to operate near the linear region. In the following, the system performance has been shown for different values of IBO. To verify the analytical results, different sets of coefficients for different IBO are used to characterise the nonlinear HPA with memory.[3]

A. SDNR SIMULATION

In this section, we analyse the impact of nonlinear HPA on CA-OFDM signals in the absence of channel fading and AWGN effects, i.e., $N_o = 0$. This leads to $SDNR_{q,k} = \frac{P_b\left|\mu^j_{q,k}\right|^2}{\sigma^2_{\eta^j_{q,k}}}$, where $SDNR_{q,k}$ is the signal-to-distortion-noise ratio at k^{th} subcarrier on q^{th} frequency band.

Fig. 3 and Fig. 4 shows the impact of $\mu^j_{q,k}$ and $\sigma^2_{\eta^j_{q,k}}$, respectively, on different subcarriers of a CA-OFDM system. The theoretical and simulation results coincide at each subcarrier,

[3]The number of coefficients for each IBO is between 40-120 depending upon the number of aggregated carriers and HPA parameters, however due to space constraint they are not shown in this paper. Interested readers can refer https://www.iiitd.edu.in/~wirocomm/resources/coefficients_MB_GMP.xlsx

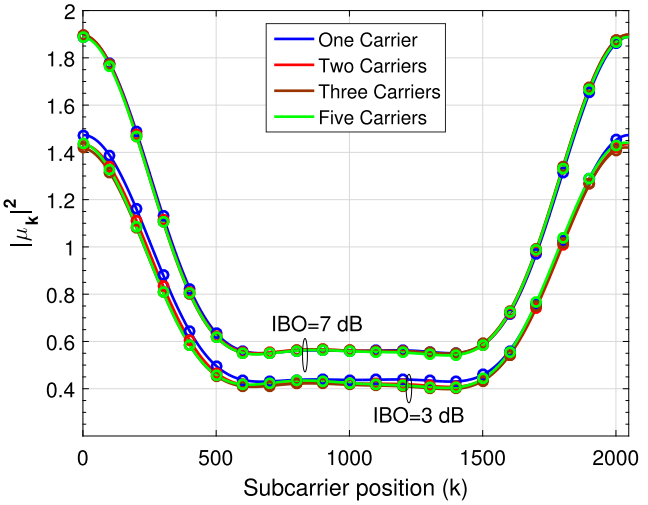

FIGURE 3. Analytical (solid lines) and simulation (marker points) results of the complex attenuation factor for each subcarrier of different CA-OFDM signals for 16 QAM.

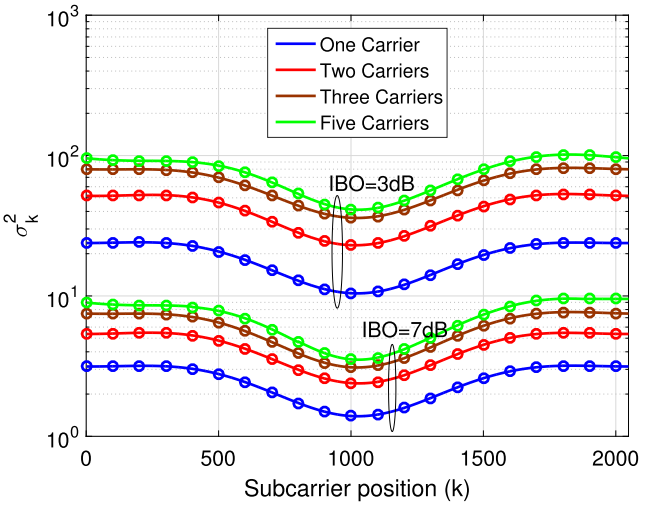

FIGURE 4. Analytical (solid lines) and simulation (marker points) results of variance of nonlinear noise for each subcarrier of different CA-OFDM signals for 16 QAM.

which validates the derived mathematical expressions. It can also be observed that both $\mu^j_{q,k}$ and $\sigma^2_{\eta^j_{q,k}}$ are a function of number of aggregated bands. As the number of aggregated bands increases in CA-OFDM signal, $\mu^j_{q,k}$ decreases whereas $\sigma^2_{\eta^j_{q,k}}$ increases which deteriorate the received SNR, which supports the discussion in Section III.

From Fig. 3, it can also be observed that with increase in IBO, the value of $\mu^j_{q,k}$ increases. This is due to fact that

$$EVM_q = \frac{(N_o)^{N_R-N_T+1}}{\Gamma\left(N_R-N_T+\frac{1}{2}\right)(N_R-N_T)!N_TN}\sum_{j=0}^{N_T-1}\sum_{k=0}^{N-1}\frac{U\left(N_R-N_T+\frac{1}{2},N_R-N_T+2,\frac{N_o}{\Phi_k\sigma^2_{\eta^j_{q,k}}}\right)}{\sqrt{\Phi_k}\left|\mu^j_{q,k}\right|\left(\Phi_k\sigma^2_{\eta^j_{q,k}}\right)^{N_R-N_T+\frac{1}{2}}}. \tag{35}$$

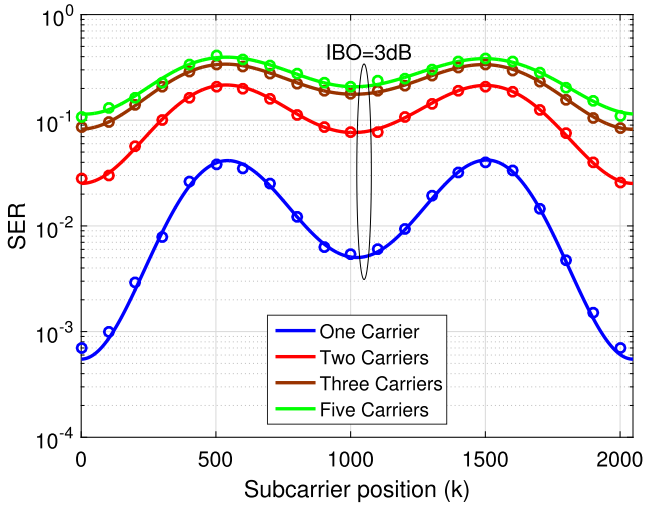

FIGURE 5. Analytical (solid lines) and simulation (marker points) results of average SER for each subcarrier of different CA-OFDM signals without AWGN for 16 QAM and IBO=3dB.

the increase in IBO forces HPA to operate in linear region which increases the value of linear coefficients and reduces the value of nonlinear coefficients. As a result, the impact of in-band and cross-modulation terms reduces which improves the system performance. Moreover, at high IBO (say 7dB), the value of $\mu^{j}_{q,k}$ for different number of aggregated bands are approximately same because of the low impact of nonlinear coefficients.

It is also noticeable from Fig. 3 and Fig. 4 that the complex attenuation and variance of nonlinear noise affects each subcarrier differently. The subcarriers located towards the end of the spectrum have considerable attenuation than other subcarriers while the variance of nonlinear noise is less in middle subcarriers than others, due to which middle and edge subcarriers are less vulnerable to nonlinear distortion

Fig. 5 shows the impact of nonlinear distortion on the SER of each subcarrier of CA-OFDM signals when $N_o = 0$. From Fig. 5, it can be observed that the SER in each subcarrier is different due to the multi-band nonlinear distortion. Specifically, subcarriers in the middle and edge are less prone to symbol errors than the other subcarriers, which is also apparent from Fig. 3 and Fig. 4.

From above discussion, it is quite obvious that by judicious subcarrier mapping and allocation, the performance of CA-MIMO-OFDM system in presence of nonlinear HPA can be optimized.

B. CA-MIMO-OFDM SIMULATION

In this section, we evaluate the symbol error performance of CA-MIMO-OFDM system impaired by nonlinear HPAs. The MIMO channel is characterised by the six delay taps with uniform power delay profile [14]. The number of subcarriers in each OFDM signal is $N = 2048$ with cyclic prefix of length $Ng = 512$. Each subcarrier contain symbols from a 16-QAM constellation. The simulation are averaged over 10^6 iterations, where for each iteration the data symbols and the channel are randomly and independently generated.

TABLE 1. Transmit signal EVM (%) for 16-QAM CA-OFDM signal with N = 2048.

Number of Carriers	One	Two	Three	Five
IBO=1dB	21.15	38.24	50.74	59.65
IBO=3dB	16.71	25.34	31.60	34.31
IBO=5dB	12.03	17.37	19.56	20.92
IBO=7dB	8.54	11.21	11.97	13.84

Fig. 6 shows the average SER performance as a function of AWGN SNR, i.e., P_{av}/N_o and IBO for different CA-MIMO-OFDM. As an ideal performance benchmark, system performance with linear HPA is also plotted. The impact of nonlinear distortion on the received signal decreases with increase in IBO. It can also be seen that SER performance of CA-MIMO-OFDM system improves with increase in SNR up to some extent, after that increase in SNR has no significant impact on the SER performance. This is due to fact that at high SNR, say SNR $>$ 40 dB, the AWGN effect reduces and only nonlinear distortion caused by HPA affects the performance. Further, on increasing the value of IBO, the impact of nonlinear distortion can be reduced and the system performance of CA-MIMO-OFDM with nonlinear HPA approaches to linear system. From Fig. 6(a) and 6(c), it can be observed that even for same IBO, there is considerable performance difference when the number of aggregated carriers is switched from three to five carriers in 2x2 CA-MIMO-OFDM system. This strengthen the fact that the increase in number of aggregated carriers leads multi-band HPA to operate more towards nonlinear region which further degrades the error performance of CA-MIMO-OFDM system.

The impact of different diversity gain $(N_r - N_t + 1)$ on the performance of CA-MIMO-OFDM systems is illustrated in Fig. 7. Although increase in diversity gain improves the SER performance, however it is limited to the low SNR regime and high values of IBO as shown in Fig. 7(a). At higher SNR as shown in Fig. 7(b), there is no significant impact of diversity gain at low IBO, however SER performance improves with diversity gain (up to order of 4) at higher IBO.

It can also be inferred from the above figures that for low SNR, SER improves with increase in AWGN SNR and diversity gain as AWGN and diversity outweigh the effects of nonlinearity, however the system performance is still lower than linear system. In high SNR regime, the nonlinear noise dominates AWGN and diversity gain which leads to irreducible error floor. This justifies the discussion in Section IV.

C. EVM ANALYSIS

In this section, the EVM performance of a nonlinear CA-MIMO-OFDM system has been evaluated for the simulation setup defined in Section VI-B.

The transmit signal EVM can be defined as $\text{EVM}_q^{TX} = \frac{1}{N}\sum_{N}^{k=0}\sqrt{\frac{1}{SDNR_{q,k}}}$. Table 1 provides useful insights on the

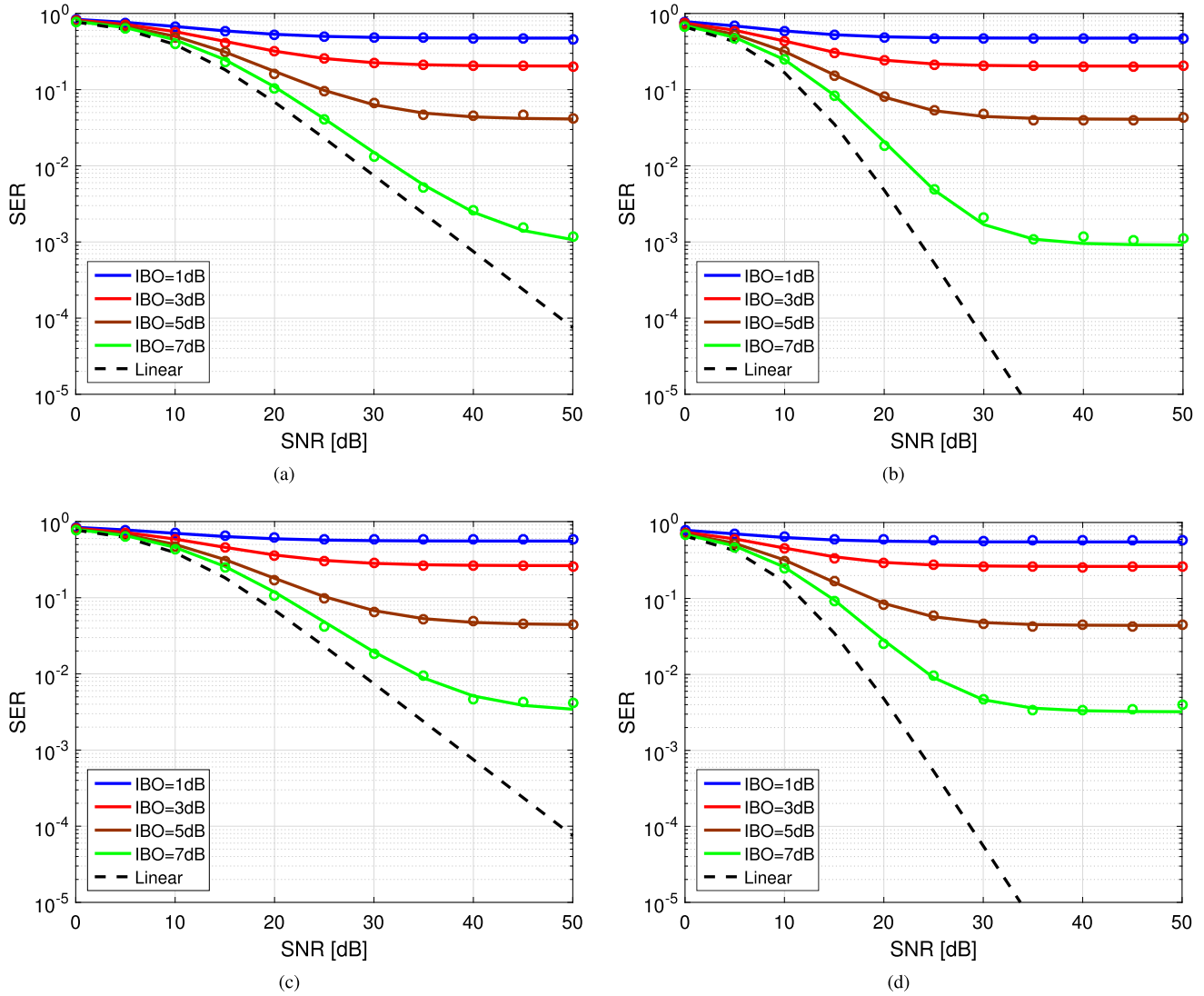

FIGURE 6. Analytical (solid lines) and simulation (marker points) results of average SER of different CA-MIMO-OFDM system in Rayleigh fading channel for 16-QAM, N = 2048. (a) Average SER of 2x2 CA-MIMO-OFDM system with three carriers. (b) Average SER of 3x2 CA-MIMO-OFDM system with three carriers. (c) Average SER of 2x2 CA-MIMO-OFDM system with five carriers. (d) Average SER of 3x2 CA-MIMO-OFDM system with five carriers.

effect of different number of aggregated bands on the transmit signal EVM. It can be observed that EVM increases as the number of aggregated bands increases. On operating nonlinear HPA with higher back-off, EVM can be maintained within a tolerance level. As per 3GPP specifications TS 136.101 [34] and TS 136.104 [35], maximum transmit signal EVM for 16-QAM is 12.5%. It is quite obvious that higher IBO is required, if there are more number of aggregated bands, in order to keep the transmit signal EVM under 3GPP specification. This observation will be quite useful when estimating the power efficiency- energy consumption trade-off while designing a CA LTE-A network. More the aggregated bands better will be throughput, however it may reduce the power efficiency of the network. The impact of AWGN SNR, i.e., P_{av}/N_o on the average EVM at receiver for different values of IBO for 2x2 CA-MIMO-OFDM system with three and five aggregated carriers is shown in Fig. 8. Good agreement between analytical and simulation results of EVM at receiver validate the accuracy of the closed form expression of EVM derived in Section V. In low SNR regime, the value of EVM is too high due to the composite effect of nonlinear noise, channel fading and AWGN. The increase in SNR reduces the impact of channel fading and AWGN which results in low EVM. However, the value of EVM at the receiver saturates to the transmit signal EVM in high SNR regime due to the nonlinear distortion caused by HPA. This concludes that generalised expression of EVM can be used to calculate EVM at both transmitter and receiver.

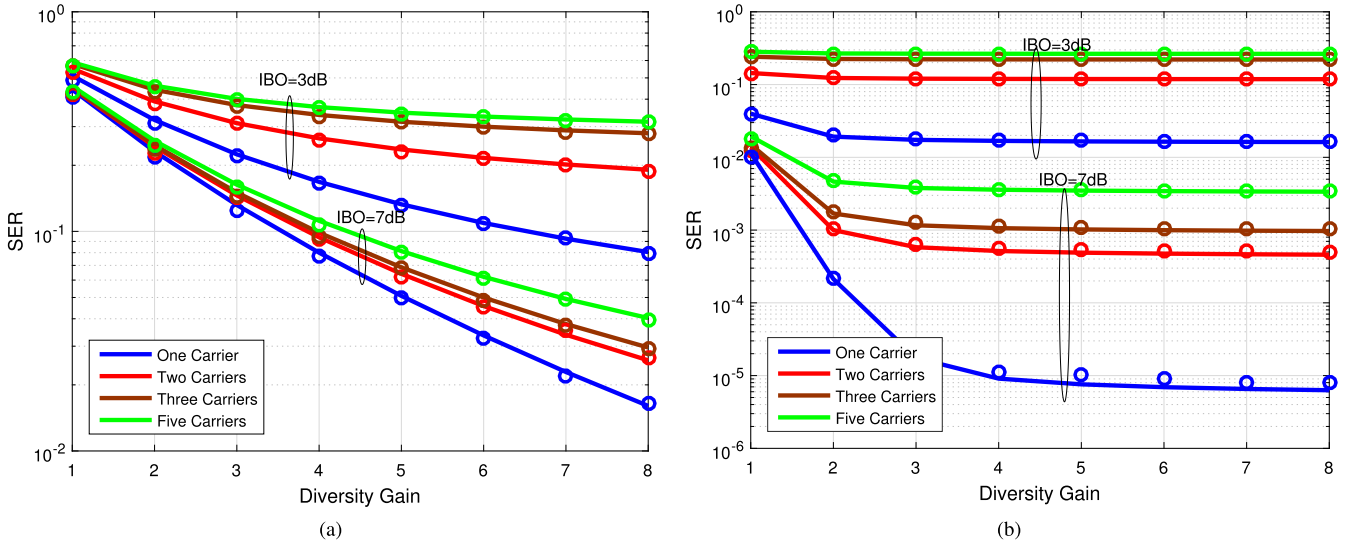

FIGURE 7. Analytical (solid lines) and simulation (marker points) results of average SER for different diversity gain of CA-MIMO-OFDM system in Rayleigh fading channel for 16-QAM, N = 2048. (a) Average SER at AWGN SNR = 10dB. (b) Average SER at AWGN SNR = 30dB.

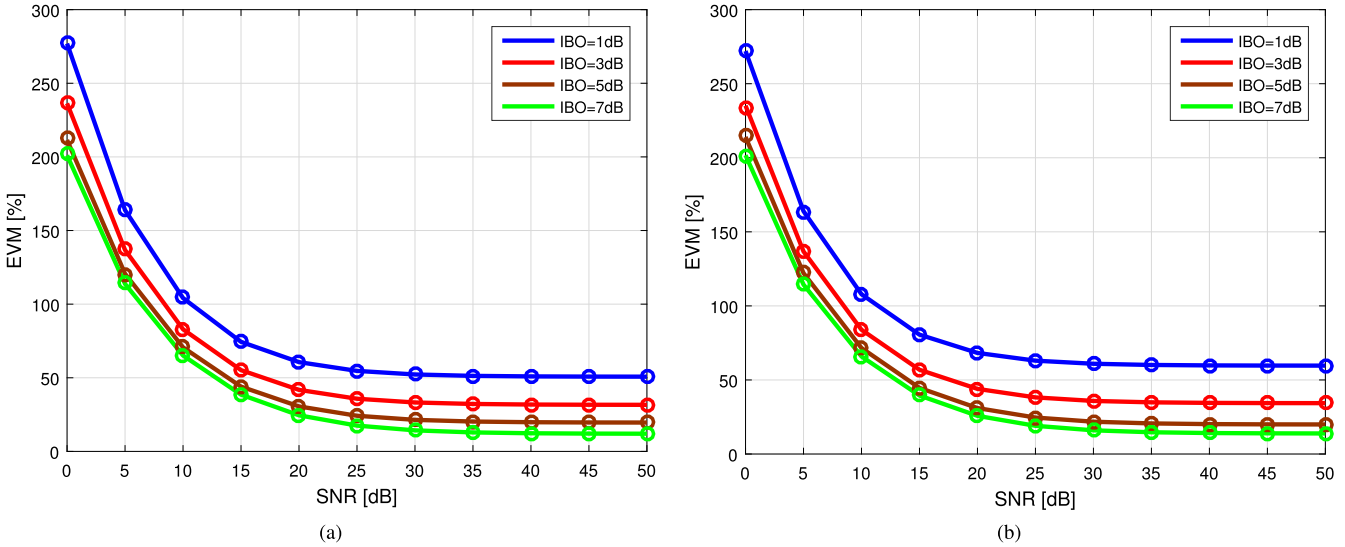

FIGURE 8. Analytical (solid lines) and simulation (marker points) results of average EVM for 2x2 CA-MIMO-OFDM system in Rayleigh fading channel for 16-QAM, N = 2048. (a) EVM (%) for three carriers. (b) EVM (%) for five carriers.

VII. CONCLUSION

In this paper, we investigated the performance of CA LTE-A system in the presence of nonlinear HPA for a multi-path Rayleigh fading MIMO channel. The nonlinear behavior of HPA has been modeled using a MB-GMP model. It has been shown that nonlinear distortions at the output of a HPA for a CA-MIMO-OFDM system can be canonically characterised in terms of complex attenuation factor and additive zero mean Gaussian nonlinear noise. Closed-form generalised expressions of complex attenuation factor and nonlinear noise are derived that are applicable for any number of aggregated bands with any nonlinearity and memory depth. From the expressions, a complete analytical approach is presented to obtain the received SNR, SER and EVM for each subcarrier of CA-MIMO-OFDM systems.

It was also observed that the nonlinear distortion caused by multi-band HPA increases with increase in number of aggregated bands which diminishes the gain due to diversity and SNR. Further, the nonlinear distortion impacts each subcarrier of the received CA-OFDM signal differently. The nonlinear distortions can be alleviated to certain extent by increasing the IBO. Therefore, by judicious subcarrier mapping and appropriate selection of IBO, the performance of a CA-MIMO-OFDM system can be optimized in presence of nonlinear HPA. The derived analytical results will be useful when estimating a power efficiency and energy consumption

trade-off while designing CA LTE-A based wireless systems without performing extensive simulation or tedious experiments.

APPENDIX A
DECOMPOSITION OF RECEIVED SIGNAL

Multiply (12) by $b^{j*}_{q,k}$, taking the expectation of the resultant term with an assumption that $\mu^j_{q,k}$ is an unknown parameter. Thus, we have

$$\mathrm{E}[s^j_{q,k} b^{j*}_{q,k}] = \mu^j_{q,k} P_b \tag{36}$$

Substituting $s^j_{q,k}$ from (12) and $b^{j*}_{q,k}$ by its IDFT,

$$\begin{aligned}
&\mathrm{E}[s^j_{q,k} b^{j*}_{q,k}] \\
&= E\left[\sum_{n=0}^{N-1}\sum_{p_1=1}^{P}\sum_{p_2=1}^{p_1}\cdots\sum_{p_Q=1}^{p_{Q-1}}\sum_{g=-G}^{G}\right. \\
&\quad\times \alpha^j_{p_1,p_2,\cdots,p_Q,k,g} x^j_q[n+g]\left|x^j_1[n]\right|^{p_1-p_2}\cdots\left|x^j_Q[n]\right|^{p_Q-1} \\
&\quad\left.\times e^{-j2\pi k(n+g)/N}\sum_{u=0}^{N-1} x^{j*}_q[u] e^{j2\pi uk/N}\right]
\end{aligned} \tag{37}$$

As stated earlier, $x^j_q[n]$ can be approximated to Gaussian random process using CLT with zero mean and variance $P_{av} = P_b/N$. Hence, any function of $x^j_q[n_1]$ and $x^j_q[n_2]$ with $n_1 \neq n_2$ are jointly Gaussian. Moreover, two different components of inverse discrete Fourier transform (IDFT) of i.i.d. random sequence are uncorrelated [14]. Hence, $x^j_q[n_1]$ and $x^j_q[n_2]$ are uncorrelated. Since, $x^j_q[n_1]$ and $x^j_q[n_2]$ are jointly Gaussian and uncorrelated, therefore they are independent as well. Moreover, $\left|x^j_q[n]\right|$ is Rayleigh distributed random variable whose central moment is known.

In (37), if $n+g \neq u$ the expected value is zero, therefore we have

$$\begin{aligned}
&\mathrm{E}[s^j_{q,k} b^{j*}_{q,k}] \\
&= \sum_{n=0}^{N-1}\sum_{p_1=1}^{P}\sum_{p_2=1}^{p_1}\cdots\sum_{p_Q=1}^{p_{Q-1}}\sum_{g=-G}^{G}\alpha^j_{p_1,p_2,\cdots,p_Q,k,g} \\
&\quad\times \mathrm{E}\left[\left|x^j_q[n+g]\right|^2\left|x^j_1[n]\right|^{p_1-p_2}\cdots\left|x^j_Q[n]\right|^{p_Q-1}\right]
\end{aligned} \tag{38}$$

After some manipulations and using (36) and (38), $\mu^j_{q,k}$ can be expressed as

$$\begin{aligned}
\mu^j_{q,k} &= \sum_{p_1=1}^{P}\sum_{p_2=1}^{p_1}\cdots\sum_{p_Q=1}^{p_{Q-1}}\left(\frac{P_b}{N}\right)^{\frac{p_1-1}{2}}\left(\alpha^j_{p_1,p_2,\cdots,p_Q,k,0}\right. \\
&\quad\times\Gamma\left(1+\frac{p_1-p_2}{2}\right)\cdots\Gamma\left(1+\frac{p_q-p_{q+1}+2}{2}\right) \\
&\quad\cdots\Gamma\left(1+\frac{p_Q-1}{2}\right)+\sum_{\substack{g=-G\\ g\neq 0}}^{G}\alpha^j_{p_1,p_2,\cdots,p_Q,k,g}\Gamma(2) \\
&\quad\left.\times\Gamma\left(1+\frac{p_1-p_2}{2}\right)\cdots\Gamma\left(1+\frac{p_Q-1}{2}\right)\right)
\end{aligned} \tag{39}$$

As a result, $s^j_{q,k}$ can be expressed as

$$s^j_{q,k} = \mu^j_{q,k} b^j_{q,k} + \eta^j_{q,k} \tag{40}$$

where $\eta^j_{q,k}$ is a nonlinear noise.

APPENDIX B
MEAN OF NONLINEAR NOISE

The mean of nonlinear noise $\eta^j_{q,k}$ can be expressed as

$$\mathrm{E}[\eta^j_{q,k}] = \mathrm{E}[s^j_{q,k}] - \mu^j_{q,k}\mathrm{E}[b^j_{q,k}] \tag{41}$$

Since, $b^j_{q,k}$ has zero mean, i.e., $\mathrm{E}[b^j_{q,k}] = 0$. Thus, we have

$$\mathrm{E}[\eta^j_{q,k}] = \mathrm{E}[s^j_{q,k}] \tag{42}$$

Using (12) and replacing $x^j_1[n+g]$ by its IDFT, we have

$$\begin{aligned}
s^j_{q,k} &= \sum_{n=0}^{N-1}\sum_{p_1=1}^{P}\sum_{p_2=1}^{p_1}\cdots\sum_{p_Q=1}^{p_{Q-1}}\sum_{m=0}^{M-1}\sum_{g=-G}^{G}\alpha^j_{p_1,p_2,\cdots,p_Q,k,g} \\
&\quad\times\left|x^j_1[n]\right|^{p_1-p_2}\cdots\left|x^j_Q[n]\right|^{p_Q-1} e^{-j2\pi k(n+g+m)/N} \\
&\quad\times\frac{1}{N}\sum_{u=0}^{N-1} b^j_{t,u} e^{j2\pi u(n+g)/N}
\end{aligned} \tag{43}$$

On substituting IDFT of $b^j_{t,u}$ and taking the expectation of $s^j_{q,k}$, we have

$$\begin{aligned}
\mathrm{E}[s^j_{q,k}] &= \sum_{n=0}^{N-1}\sum_{p_1=1}^{P}\sum_{p_2=1}^{p_1}\cdots\sum_{p_Q=1}^{p_{Q-1}}\sum_{g=-G}^{G}\sum_{u=0}^{N-1}\alpha^j_{p_1,p_2,\cdots,p_Q,k,g} \\
&\quad\frac{1}{N}\sum_{v=0}^{N-1}\mathrm{E}\left[x^j_q[v]\left|x^j_1[n]\right|^{p_1-p_2}\cdots\left|x^j_Q[n]\right|^{p_Q-1}\right] \\
&\quad e^{-j2\pi k(n+g)/N} e^{j2\pi u(n+g)/N} e^{-j2\pi uv/N}
\end{aligned} \tag{44}$$

If $v \neq n$, then expectation will be zero, then we have

$$\begin{aligned}
\mathrm{E}[s^j_{q,k}] &= \sum_{n=0}^{N-1}\sum_{p_1=1}^{P}\sum_{p_2=1}^{p_1}\cdots\sum_{p_Q=1}^{p_{Q-1}}\sum_{g=-G}^{G}\sum_{u=0}^{N-1}\alpha^j_{p_1,p_2,\cdots,p_Q,k,g} \\
&\quad\times\frac{1}{N}\mathrm{E}\left[x^j_q[n]\left|x^j_1[n]\right|^{p_1-p_2}\cdots\left|x^j_Q[n]\right|^{p_Q-1}\right] \\
&\quad\times e^{-j2\pi k(n+g)/N} e^{j2\pi ug/N}
\end{aligned} \tag{45}$$

We know that all the OFDM signals $x^j_q[n]$ independent to each other, we can rewrite the above equation as

$$\begin{aligned}
\mathrm{E}[s^j_{q,k}] &= \sum_{n=0}^{N-1}\sum_{p_1=1}^{P}\sum_{p_2=1}^{p_1}\cdots\sum_{p_Q=1}^{p_{Q-1}}\sum_{g=-G}^{G}\sum_{u=0}^{N-1}\alpha^j_{p_1,p_2,\cdots,p_Q,k,g} \\
&\quad\times\frac{1}{N}\mathrm{E}\left[\left|x^j_1[n]\right|^{p_1-p_2}\right]\cdots\mathrm{E}\left[x^j_q[n]\left|x^j_q[n]\right|^{p_q-p_{q+1}}\right] \\
&\quad\cdots\mathrm{E}\left[\left|x^j_Q[n]\right|^{p_Q-1}\right] e^{-j2\pi k(n+g)/N} e^{j2\pi ug/N}
\end{aligned} \tag{46}$$

Since, $x^j_q[n]$ is circularly symmetric complex-valued Gaussian random variable and $|x^j_q[n]|^{\hat{p}}$ is a random positive

$$\mathrm{E}\left[\left|s_{q,k}^{j}\right|^{2}\right]=\frac{1}{N^{2}}\sum_{n=0}^{N-1}\sum_{p_1=1}^{P}\sum_{p_2=1}^{p_1}\cdots\sum_{p_Q=1}^{p_{Q-1}}\sum_{g=-G}^{G}\sum_{u=0}^{N-1}\sum_{v=0}^{N-1}\sum_{n'=0}^{N-1}\sum_{p'_1=1}^{P}\sum_{p'_2=1}^{p'_1}\cdots\sum_{p'_Q=1}^{p'_{T-1}}\sum_{g'=-G}^{G}\sum_{u'=0}^{N-1}\sum_{v'=0}^{N-1}\alpha^{j}_{p_1,p_2,\cdots,p_Q,k,g}$$
$$\times\,{\alpha^{j}_{p'_1,p'_2,\cdots,p'_Q,k,g'}}^{*}e^{-j2\pi k(n+g)/N}e^{j2\pi u(n+g)/N}e^{-j2\pi uv/N}e^{j2\pi k(n'+g')/N}e^{j2\pi u'v'/N}e^{-j2\pi u'(n'+g')/N}$$
$$\times\,E\left[x_q^{j}[v]\left|x_1^{j}[n]\right|^{p_1-p_2}\cdots\left|x_Q^{j}[n]\right|^{p_Q-1}x_q^{j}[v']^{*}\left|x_1^{j}[n']\right|^{p'_1-p'_2}\cdots\left|x_Q^{j}[n']\right|^{p'_Q-1}\right] \tag{51}$$

number, where $\hat{p}=p_q-p_{q+1}$. Therefore, the new random variable $x_q^j[n]|x_q^j[n]|^{\hat{p}}$ is also circularly symmetric and its mean is zero. To prove this mathematically, we have $z=\sqrt{real\left(x_{q,k}^{j}[n]\right)^2+imag\left(x_{q,k}^{j}[n]\right)^2}$ and $\theta=\tan^{-1}\frac{imag\left(x_{q,k}^{j}[n]\right)}{real\left(x_{q,k}^{j}[n]\right)}$ where z and θ are amplitude and phase of $x_q^j[n]$ and are independent with Rayleigh and uniform distribution, respectively. Their joint distribution is

$$f_{z,\theta}(z,\theta)=\frac{z}{2\pi\sigma^2}e^{-\frac{z}{2\sigma^2}} \tag{47}$$

where σ^2 is a common variance of $real(x_{q,k}^j[n])$ and $imag(x_{q,k}^j[n])$. Thus, the expectation of $x_q^j[n]|x_q^j[n]|^{\hat{p}}$ can be expressed as

$$\mathrm{E}\left[x_q^{j}[n]\left|x_q^{j}[n]\right|^{q}\right]=\int_{-\pi}^{\pi}\int_{0}^{\infty}ze^{j\theta}z^{p}f_{z,\theta}(z,\theta)dzd\theta$$
$$=\int_{0}^{\infty}\frac{z^{q+1}}{2\pi\sigma^2}e^{-\frac{z}{2\sigma^2}}dr\int_{-\pi}^{\pi}e^{j\theta}d\theta=0 \tag{48}$$

Using (42), (46) and (48), it is proved that nonlinear noise has zero mean, i.e.,

$$\mathrm{E}[\eta_{q,k}^{j}]=\mathrm{E}[s_{q,k}^{j}]=0 \tag{49}$$

APPENDIX C
VARIANCE OF NONLINEAR NOISE

The variance of nonlinear noise can be given as

$$\sigma^2_{\eta_{q,k}^{j}}=\mathrm{E}\left[\left|\eta_{q,k}^{j}\right|^{2}\right]=\mathrm{E}\left[\left|s_{q,k}^{j}\right|^{2}\right]-P_b\left|\mu_{q,k}^{j}\right|^{2} \tag{50}$$

Using (43) and IDFT of $b_{t,u}^j$, we have (51), as shown at the top of this page.

If $v\neq v'$, then the expectation value leads to zero,

$$\mathrm{E}\left[\left|s_{q,k}^{j}\right|^{2}\right]=\frac{1}{N^{2}}\sum_{p_1=1}^{P}\sum_{p_2=1}^{p_1}\cdots\sum_{p_Q=1}^{p_{Q-1}}\sum_{g=-G}^{G}\sum_{p'_1=1}^{P}\sum_{p'_2=1}^{p'_1}\cdots\sum_{p'_Q=1}^{p'_{T-1}}$$
$$\times\sum_{g'=-G}^{G}\alpha^{j}_{p_1,p_2,\cdots,p_Q,k,g}{\alpha^{j}_{p'_1,p'_2,\cdots,p'_Q,k,g'}}^{*}$$
$$\times\,\rho^{j}_{p_1,p_2,\cdots,p_Q,g,p'_1,p'_2,\cdots,p'_Q,g',k} \tag{52}$$

where

$$\rho^{j}_{p_1,p_2,\cdots,p_Q,g,p'_1,p'_2,\cdots,p'_Q,g',k}$$
$$=\sum_{n=0}^{N-1}\sum_{u=0}^{N-1}\sum_{v=0}^{N-1}\sum_{n'=0}^{N-1}\sum_{u'=0}^{N-1}E\left[\left|x_q^{j}[v]\right|^{2}\left|x_1^{j}[n]\right|^{p_1-p_2}\right.$$
$$\left.\times\cdots\left|x_Q^{j}[n]\right|^{p_Q-1}\left|x_1^{j}[n']\right|^{p'_1-p'_2}\cdots\left|x_Q^{j}[n']\right|^{p'_Q-1}\right]$$
$$\times\,e^{j2\pi u(n+g)/N}e^{-j2\pi u'(n'+g')/N}e^{-j2\pi v(u-u')/N}$$
$$\times\,e^{-j2\pi k(n+g-n'-g')/N}$$
$$\times\,\rho^{j}_{p_1,p_2,\cdots,p_Q,g,p'_1,p'_2,\cdots,p'_Q,g',k}=\rho_1^j+\rho_2^j+\rho_3^j+\rho_4^j+\rho_5^j \tag{53}$$

There are five possible cases depending upon the value of v, n and n'.

If $v=n=n'$, we have

$$\rho_1^j=N^3\delta(g)\delta(g')\Gamma\left(1+\frac{p_1-p_2+p'_1-p'_2}{2}\right)$$
$$\cdots\Gamma\left(1+\frac{p_q-p_{q+1}+p'_q-p'_{q+1}+2}{2}\right)$$
$$\cdots\Gamma\left(1+\frac{p_Q+p'_Q-2}{2}\right)\left(\frac{P_b}{N}\right)^{\frac{p_1+p'_1}{2}} \tag{54}$$

If $v=n\neq n'$, we have

$$\rho_2^j=N^3\delta(g)\left(1-\delta(g')\right)\Gamma\left(1+\frac{p_1-p_2}{2}\right)\Gamma\left(1+\frac{p'_1-p'_2}{2}\right)$$
$$\cdots\Gamma\left(1+\frac{p_q-p_{q+1}+2}{2}\right)\Gamma\left(1+\frac{p'_q-p'_{q+1}}{2}\right)$$
$$\cdots\Gamma\left(1+\frac{p_Q-1}{2}\right)\Gamma\left(1+\frac{p'_Q-1}{2}\right)\left(\frac{P_b}{N}\right)^{\frac{p_1+p'_1}{2}} \tag{55}$$

If $v=n'\neq n$, we have

$$\rho_3^j=N^3\delta(g')\left(1-\delta(g)\right)\Gamma\left(1+\frac{p_1-p_2}{2}\right)\Gamma\left(1+\frac{p'_1-p'_2}{2}\right)$$
$$\cdots\Gamma\left(1+\frac{p_q-p_{q+1}}{2}\right)\Gamma\left(1+\frac{p'_q-p'_{q+1}+2}{2}\right)$$
$$\cdots\Gamma\left(1+\frac{p_Q-1}{2}\right)\Gamma\left(1+\frac{p'_Q-1}{2}\right)\left(\frac{P_b}{N}\right)^{\frac{p_1+p'_1}{2}} \tag{56}$$

If $v \neq n = n'$, we have

$$\rho_4^j = N^3 (1-\delta(g)) \left(1-\delta(g')\right) \delta(g-g') \Gamma(2) \times \Gamma\left(1+\frac{p_1-p_2+p_1'-p_2'}{2}\right) \cdots \Gamma\left(1+\frac{p_q-p_{q+1}+p_q'-p_{q+1}'}{2}\right) \cdots \Gamma\left(1+\frac{p_Q+p_Q'-2}{2}\right) \left(\frac{P_b}{N}\right)^{\frac{p_1+p_1'}{2}} \quad (57)$$

If $v \neq n \neq n'$, we have

$$\rho_5^j = N^3 (1-\delta(g)) \left(1-\delta(g')\right) \left(1-\delta(g-g')\right) \Gamma(2) \times \Gamma\left(1+\frac{p_1-p_2}{2}\right) \Gamma\left(1+\frac{p_1'-p_2'}{2}\right) \cdots \Gamma\left(1+\frac{p_q-p_{q+1}}{2}\right) \Gamma\left(1+\frac{p_q'-p_{q+1}'}{2}\right) \cdots \Gamma\left(1+\frac{p_Q-1}{2}\right) \Gamma\left(1+\frac{p_Q'-1}{2}\right) \left(\frac{P_b}{N}\right)^{\frac{p_1+p_1'}{2}} \quad (58)$$

REFERENCES

[1] S. Parkvall, A. Furuskar, and E. Dahlman, "Evolution of LTE toward IMT-advanced," *IEEE Commun. Mag.*, vol. 49, no. 2, pp. 84–91, Feb. 2011.

[2] W. Wang, Z. Zhang, and A. Huang, "Spectrum aggregation: Overview and challenges," *Netw. Protocols Algorithms*, vol. 2, no. 1, pp. 184–196, 2010.

[3] Z. Shen, A. Papasakellariou, J. Montojo, D. Gerstenberger, and F. Xu, "Overview of 3GPP LTE-advanced carrier aggregation for 4G wireless communications," *IEEE Commun. Mag.*, vol. 50, no. 2, pp. 122–130, Feb. 2012.

[4] J. Liu and W. Xiao, "Advanced carrier aggregation techniques for multi-carrier ultra-dense networks," *IEEE Commun. Mag.*, vol. 54, no. 7, pp. 61–67, Jul. 2016.

[5] Y. Wu and W. Y. Zou, "Orthogonal frequency division multiplexing: A multi-carrier modulation scheme," *IEEE Trans. Consum. Electron.*, vol. 41, no. 3, pp. 392–399, Aug. 1995.

[6] Y. G. Li, J. H. Winters, and N. R. Sollenberger, "MIMO-OFDM for wireless communications: Signal detection with enhanced channel estimation," *IEEE Trans. Commun.*, vol. 50, no. 9, pp. 1471–1477, Sep. 2002.

[7] P. Yen, H. Minn, and C. C. Chong, "PAPR reduction for bandwidth-aggregated OFDM and SC-FDMA systems," in *Proc. IEEE Wireless Commun. Netw. Conf.*, Mar. 2011, pp. 1363–1368.

[8] P. Yen and H. Minn, "Low complexity PAPR reduction methods for carrier-aggregated MIMO OFDMA and SC-FDMA systems," *EURASIP J. Wireless Commun. Netw.*, vol. 2012, no. 1, pp. 1–13, 2012.

[9] P. Banelli, "Theoretical analysis and performance of OFDM signals in nonlinear fading channels," *IEEE Trans. Wireless Commun.*, vol. 2, no. 2, pp. 284–293, Mar. 2003.

[10] V. A. Bohara and S. H. Ting, "Theoretical analysis of OFDM signals in nonlinear polynomial models," in *Proc. 6th Int. Conf. Inf. Commun. Signal Process.*, Dec. 2007, pp. 1–5.

[11] M. H. Madani, A. Abdipour, and A. Mohammadi, "Analysis of performance degradation due to non-linearity and phase noise in orthogonal frequency division multiplexing systems," *IET Commun.*, vol. 4, no. 10, pp. 1226–1237, Jul. 2010.

[12] V. A. Bohara and S. H. Ting, "Analysis of OFDM signals in nonlinear high power amplifier with memory," in *Proc. IEEE Int. Conf. Commun.*, May 2008, pp. 3653–3657.

[13] V. A. Bohara and S. H. Ting, "Analytical performance of orthogonal frequency division multiplexing systems impaired by a non-linear high-power amplifier with memory," *IET Commun.*, vol. 3, no. 10, pp. 1659–1666, Oct. 2009.

[14] H. Hemesi, A. Abdipour, and A. Mohammadi, "Analytical modeling of MIMO-OFDM system in the presence of nonlinear power amplifier with memory," *IEEE Trans. Commun.*, vol. 61, no. 1, pp. 155–163, Nov. 2013.

[15] J. Qi and S. Aissa, "On the power amplifier nonlinearity in MIMO transmit beamforming systems," *IEEE Trans. Commun.*, vol. 60, no. 3, pp. 876–887, Mar. 2012.

[16] I. Iofedov and D. Wulich, "MIMO–OFDM with nonlinear power amplifiers," *IEEE Trans. Commun.*, vol. 63, no. 12, pp. 4894–4904, Dec. 2015.

[17] P. Singhal, P. Aggarwal, and V. A. Bohara, "Analysis of carrier aggregated OFDM signals in presence of dual band power amplifiers," in *Proc. 21st Nat. Conf. Commun.*, Feb./Mar. 2015, pp. 1–6.

[18] P. Singhal, P. Aggarwal, and V. A. Bohara, "Nonlinear distortion analysis of multi-band carrier aggregated OFDM signals," in *Proc. IEEE Int. Conf. Adv. Netw. Telecommun. Syst.*, Dec. 2015, pp. 1–6.

[19] P. Aggarwal, A. Agarwal, and V. A. Bohara, "Error vector magnitude analysis for carrier aggregated OFDM signals with nonlinear HPA," in *Proc. IEEE Int. Conf. Adv. Netw. Telecommun. Syst.*, Nov. 2016, pp. 1–3.

[20] P. Aggarwal and V. A. Bohara, "Characterization of HPA using two dimensional general memory polynomial for dual band carrier aggregated MIMO-OFDM systems," in *Proc. IEEE Int. Conf. Commun.*, May 2016, pp. 1–7.

[21] A. Vaezi, A. Abdipour, A. Mohammadi, and F. M. Ghannouchi, "Analysis of MIMO-OFDM system impaired by nonlinear dual-band power amplifiers," *Analog Integr. Circuits Signal Process.*, vol. 89, no. 1, pp. 205–212, 2016. [Online]. Available: http://dx.doi.org/10.1007/s10470-016-0821-2

[22] M. S. Heutmaker, "The error vector and power amplifier distortion," in *Proc. Wireless Commun. Conf.*, Aug. 1997, pp. 100–104.

[23] K. M. Gharaibeh, K. G. Gard, and M. B. Steer, "Accurate estimation of digital communication system metrics—SNR, EVM and ρ in a nonlinear amplifier environment," in *Proc. 64th ARFTG Microw. Meas. Conf. Fall*, Dec. 2004, pp. 41–44.

[24] R. A. Shafik, M. S. Rahman, and A. R. Islam, "On the extended relationships among EVM, BER and SNR as performance metrics," in *Proc. Int. Conf. Elect. Comput. Eng.*, Dec. 2006, pp. 408–411.

[25] Z. Qijun, X. Qinghua, and Z. Wei, "A new EVM calculation method for broadband modulated signals and simulation," in *Proc. 8th Int. Conf. Electron. Meas. Instrum.*, Aug. 2007, pp. 2-661–2-665.

[26] A. Papoulis, *Probability—Random Variables and Stochastic Processes*. New York, NY, USA: McGraw-Hill, 1965.

[27] A. E. Nordsjo and L. H. Zetterberg, "Identification of certain time-varying nonlinear Wiener and Hammerstein systems," *IEEE Trans. Signal Process.*, vol. 49, no. 3, pp. 577–592, Mar. 2001.

[28] L. Ding *et al.*, "A robust digital baseband predistorter constructed using memory polynomials," *IEEE Trans. Commun.*, vol. 52, no. 1, pp. 159–165, Jan. 2004.

[29] D. R. Morgan, Z. Ma, J. Kim, M. G. Zierdt, and J. Pastalan, "A generalized memory polynomial model for digital predistortion of RF power amplifiers," *IEEE Trans. Signal Process.*, vol. 54, no. 10, pp. 3852–3860, Oct. 2006.

[30] S. A. Bassam, M. Helaoui, and F. M. Ghannouchi, "2-D digital predistortion (2-D-DPD) architecture for concurrent dual-band transmitters," *IEEE Trans. Microw. Theory Techn.*, vol. 59, no. 10, pp. 2547–2553, Oct. 2011.

[31] D. A. Gore, R. W. Heath, Jr., and A. J. Paulraj, "Transmit selection in spatial multiplexing systems," *IEEE Commun. Lett.*, vol. 6, no. 11, pp. 491–493, Nov. 2002.

[32] J. G. Proakis and M. Salehi, *Digital Communications*. New York, NY, USA: McGraw-Hill, 2008.

[33] H. Exton, *Multiple Hypergeometric Functions and Applications* (Ellis Horwood Series in Mathematics and Its Applications). New York, NY, USA: Wiley, 1976.

[34] *LTE; Evolved Universal Terrestrial Radio Access (E-UTRA); User Equipment (UE) Radio Transmission and Reception*, document 3GPP TS 36.101 ver. 12.5.0 Release 12, 2014.

[35] *LTE; Evolved Universal Terrestrial Radio Access (E-UTRA); Base Station (BS) Radio Transmission and Reception*, document 3GPP TS 36.104 ver. 11.2.0 Release 11, 2012.

PARAG AGGARWAL received the B.Tech. degree in electronics and communication from Amity University, India, in 2011, the M.Tech. degree from the Department of Information and Communication Technology, ABV-Indian Institute of Information Technology and Management, Gwalior, India, in 2014. He is currently pursuing the Ph.D. degree with the Electronics and Communication Department, Indraprastha Institute of Information Technology, Delhi, India. His research interests include digital predistortion techniques, carrier aggregation, massive MIMO, physical-layer security and cooperative wireless communication. Mr. Aggarwal was a recipient of the Best Poster Award at the IEEE Comsnets 2015 conference.

VIVEK ASHOK BOHARA received the Ph.D. degree from the School of EEE, Nanyang Technological University, Singapore, in 2011. From 2011 to 2013, he was a Postdoctoral Researcher (Marie Curie fellowship) in ESIEE Paris, University Paris-East. In 2013, he joined Indraprastha Institute of Information Technology, Delhi, where he is currently an Assistant Professor. His research interests are toward next-generation communication technologies, such as device-to-device communication, carrier aggregation, and digital predistortion algorithms. Prof. Bohara received First Prize in National Instruments ASEAN Virtual Instrumentation Applications Contest in 2007 and 2010. He was also the recipient of the Best Poster Award at the IEEE ANTS 2014 and the IEEE Comsnets 2015 and 2016 conferences.